CRYSTAL GROWTH & DESIGN

Article

Cite This: Cryst. Growth Des. 2019, 19, 5762−5767

pubs.acs.org/crystal

Liquid Salt Transport Growth of Single Crystals of the Layered Dichalcogenides MoS_2 and WS_2

F. Alex Cevallos,*[,†] Shu Guo,[†] Hoseok Heo,[‡] Giovanni Scuri,[‡] You Zhou,[‡] Jiho Sung,[‡] Takashi Taniguchi,[§] Kenji Watanabe,[§] Philip Kim,[∥] Hongkun Park,[‡] and Robert J. Cava[†]

[†]Department of Chemistry, Princeton University, Princeton, New Jersey 08542, United States

[‡]Department of Chemistry and Chemical Biology and [∥]Department of Physics, Harvard University, Cambridge, Massachusetts 02138, United States

[§]National Institute for Materials Science, 1-1 Namiki, Tsukuba 305-0044, Japan

Supporting Information

ABSTRACT: The growth of single crystals of MoS_2 and WS_2 by materials transport through a liquid salt flux made from a low-melting mixture of NaCl and CsCl is presented. The crystals are structurally characterized by single-crystal X-ray diffraction, which reveals that the 2H-MoS_2 crystals contain a very small percentage (about 3%) of 3R intergrowths and that the 2H-WS_2 crystals display less than 1% of 3R intergrowths. Characterization of the crystals by scanning electron microscopy is presented as are photoluminescence spectra of exfoliated monolayers that show that MoS_2 crystals grown by this method are superior in quality to commercially available MoS_2 crystals and equivalent to the current state of the art.

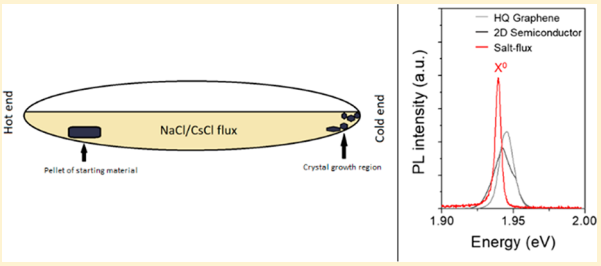

INTRODUCTION

Transition metal dichalcogenides (TMDCs) are compounds with a composition MX_2 where M is a transition metal such as tungsten or niobium, and X is a chalcogen such as sulfur, selenium, or tellurium. TMDCs have been a subject of active study for several decades due to their wide variety of observed properties,[1] including superconductivity,[2−4] charge density waves,[5,6] and photoluminescence.[7,8] In recent years, layered TMDCs such as MoS_2 have received intense focus not only due to their catalytic properties[9,10] but also for the ease with which they can be exfoliated into monolayers and the interesting properties that result.[8,11]

A significant issue that has arisen in the study of MoS_2 is the difficulty of growing large, high-quality single crystals. For example, while MoS_2 monolayers can be reliably grown using chemical vapor deposition,[12,13] bulk growth has for the most part been achieved solely by the vapor transport method,[14] which often can produce a significant number of defects and atom deficiencies, resulting in different properties under slightly altered growth conditions.[15,16] In the case of MoS_2 in particular, a substantial amount of research work has been performed on the naturally occurring mineral form of the compound, which can result in dramatically varying properties depending on a number of uncontrollable factors.[17] Bearing this in mind, as well as that natural single crystals of MoS_2 are an exhaustible and nonrenewable resource, the search for additional crystal growth methods for this compound and others is an active field of research.

Recently, Zhang et al.[18] have published an alternative approach to the growth of bulk crystals of MoS_2, using a molten metal "solution transport" method, a horizontal flux growth analogous to the more common vapor transport method[19] that has been previously successfully applied to chalcogenide and pnictide crystal growth.[20−22] The resulting crystals, grown in tin metal flux, have many desirable properties. Here, in contrast, we describe a method for crystal growth that employs a low-melting mixture of NaCl and CsCl as a salt flux for layered MoS_2, eliminating the use of a metal flux, and extend the application of this technique to the closely related compound WS_2. Characterization of thin layers of MoS_2 crystals grown in this fashion in an optical device showed excellent photoluminescent properties—better than the commercial crystals commonly employed in research on this material and equivalent to the best crystals currently reported.

EXPERIMENTAL SECTION

Polycrystalline MoS_2 was synthesized by first mixing a stoichiometric amount of molybdenum powder (99.9%, Alfa Aesar) with a 5% excess of sulfur (99.5%, Johnson Matthey). The mixture was loaded into a sealed, evacuated quartz tube and heated to 950 °C at a rate of 60 °C/h. The tube was heated for 10 days and then cooled to room temperature over 24 h. The resulting material took the form of large, loosely packed clumps of crystalline MoS_2 with a distinct "glitter" appearance, although no single crystals could be isolated of sufficient

Received: June 19, 2019
Revised: August 12, 2019
Published: September 5, 2019

DOI: 10.1021/acs.cgd.9b00785
Cryst. Growth Des. 2019, 19, 5762−5767

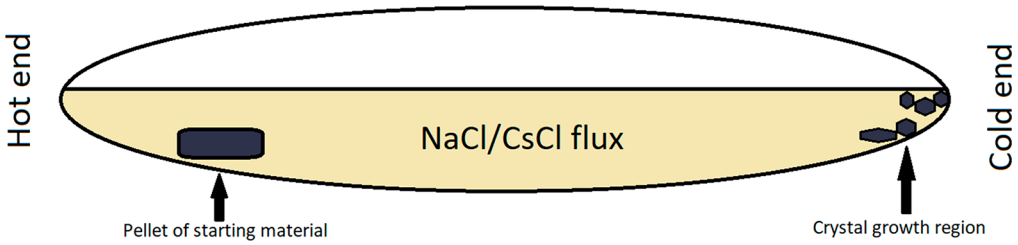

Figure 1. Cartoon schematic of the orientation used in solution-transport crystal growth.

quality for structural characterization. Polycrystalline WS_2 was similarly synthesized, with the substitution of tungsten powder (99.9%, Alfa Aesar) and a reaction temperature of 1000 °C, which resulted in a dull gray powder.

For single-crystal growth, a 100 mg pellet of polycrystalline MoS_2 or WS_2 was placed in a quartz tube of outer diameter 16 mm, wall thickness 0.8 mm, and approximately 7 cm in length (after sealing). A 10 g mixture of 38 mol % NaCl (99.0%, Alfa Aesar) and 62 mol % CsCl (99%, Alfa Aesar) was used to fill the remaining space in the tube. This salt mixture was chosen for a number of reasons; first, it forms a low-melting eutectic and is reliably liquid at temperatures above 600 °C, allowing for experimentation and crystal growth over a wide variety of temperature ranges and temperature gradients. Second, in comparison to other compounds commonly used for flux growth, such as LiCl and $AlCl_3$, both of these salts are quite air-stable and do not necessitate the use of a drybox for handling or storage. Finally, as the resulting mixture is highly water-soluble, removal and cleaning of the resulting crystals can be easily performed by washing with distilled water, without any need of mechanical separation, scraping, or centrifuging which can damage thin crystals or crystal surfaces.

The tube was sealed under a vacuum and placed in a small box furnace in a horizontal configuration, with the end containing the pellet pointed toward the back of the furnace and the growth end pointing toward the furnace door, thus using the natural temperature gradient in the furnace. The tube was then heated to 1000 °C (MoS_2) or 1100 °C (WS_2) at 90 °C/h. The molten flux covered the entire bottom of the tube, allowing for "liquid transport" analogous to the more common vapor transport crystal growth method. A diagram of this reaction orientation can be viewed in Figure 1. After 1 week, the tube was cooled to 650 °C at a rate of 2 °C/h. During cooling, the molten salt flux remained transparent, and crystals could be observed growing on the end of the tube closest to the furnace door. The tube was then removed from the furnace and quenched in a vertical orientation, in order to separate the salt flux from the resulting crystals. The crystals were then washed with distilled water in order to remove the remaining salt. The final products took the form of thin, leafy flakes of silver-colored material with a significant variation in size, although a small number of samples of both materials with a diameter of 5 mm or greater were present.

Room temperature powder X-ray diffraction (PXRD) measurements were taken using Bruker D8 Advance Eco diffractometer using Cu Kα radiation (λ = 1.5418 Å) and a LynxEye-XE detector. Single-crystal X-ray diffraction (SXRD) data were collected at 300(1) K with a Kappa Apex2 CCD diffractometer (Bruker) using graphite-monochromated Mo−Kα radiation (λ = 0.71073 Å). The raw data were corrected for background, polarization, and the Lorentz factor, and multiscan absorption corrections were applied. Finally, the structures were analyzed by the intrinsic phasing method provided by the ShelXT structure solution program[23] and refined using the ShelXL least-squares refinement package with the Olex2 program.[24] The ADDSYM algorithm in program PLATON was used to double check for possible higher symmetry.[25] Scanning electron microscopy (SEM) was performed using a Quanta 200 FEG environmental (FEI) scanning electron microscope, with an accelerating voltage of 20 keV. Energy dispersive X-ray spectroscopy (EDX) was performed using an Oxford Instruments X-Max 80 mm^2 SDD spectrometer, and data were collected and analyzed through the INCA suite of programs. Atomic force microscopy (AFM) was performed using a Bruker Dimension Icon with ScanAsyst.

For photoluminescence (PL) characterization of MoS_2, thin hexagonal boron nitride (hBN) layers (50−80 nm thick) and monolayer MoS_2 were mechanically exfoliated from bulk crystals onto SiO_2(285 nm)/Si substrates and were identified based on their optical contrast. The thickness of the selected hBN flakes was determined by atomic force microscopy measurements. Prior to exfoliation, the SiO_2/Si substrates were first ultrasonically cleaned in acetone and 2-propanol for 5 min. Following the solution-cleaning step, the substrates were subjected to further cleaning in oxygen plasma (100 W, 300 mTorr) for 10 min. Afterward, the flakes were exfoliated by the scotch-tape method. The hBN/MoS_2/hBN heterostructures were then stacked and transferred using a dry transfer method[26] onto cleaned SiO_2/Si substrates. PL measurements were carried out in a home-built confocal microscope using an objective with a numerical aperture of 0.75 under 532 nm (2.33 eV) laser excitation in a cryostat from Montana Instruments.

RESULTS AND DISCUSSION

Crystal Structure and Physical Characterization. Single-crystal X-ray diffraction patterns were measured for several planar single crystals of both MoS_2 and WS_2. The resulting crystal structures can be seen in Figure 2. Crystallographic data and atomic positions for our MoS_2 and WS_2 can be found in the Supporting Information. Single-crystal refinement of WS_2 proved unexpectedly difficult, as crystals of sufficiently small size could not be readily obtained without

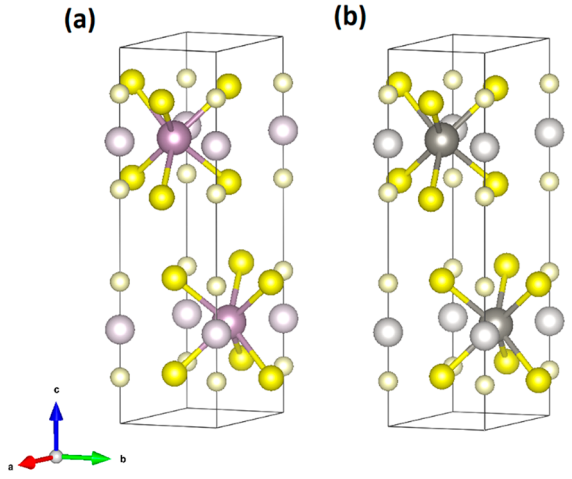

Figure 2. Crystal structures of salt-flux-grown MoS_2 and WS_2. (a) Crystal structure of MoS_2 as determined by single-crystal X-ray diffraction. Purple spheres represent Mo atoms, and yellow spheres represent S. Lighter-shaded purple and yellow spheres indicate minorly occupied Mo and S sites. (b) Crystal structure of WS_2 as determined by single-crystal X-ray diffraction. Gray spheres represent W atoms. Lighter-shaded gray and yellow spheres indicate minorly occupied W sites.

DOI: 10.1021/acs.cgd.9b00785
Cryst. Growth Des. 2019, 19, 5762−5767

introducing strain or stacking faults to the system, resulting in a slightly large residual electron density. Crystallographic analyses from the positions of sharp Bragg reflections reveal that both compounds crystallize in the hexagonal space group $P6_3/mmc$ (No. 194). Within the unit cells of both MoS_2 and WS_2, the refinements of the average structures (i.e., what the single-crystal diffraction patterns determine) show that there are two unique metal atom sites (Wyckoff sites 2*b* and 2*c*). The 2*b* site in both compounds is only slightly occupied (3.14% in MoS_2 and 0.79% in WS_2), which is an indication of the presence of stacking faults. Similarly, the unit cells of MoS_2 and WS_2 exhibit two unique S atoms sites (Wyckoff sites 4*e* and 4*f*). The 4*e* site in MoS_2 is 3.14% occupied, corresponding well to the fraction of Mo atoms in the 2*b* site. As these two values were refined independently and not fixed to each other, their agreement is significant. For WS_2, where the scattering factor for S is small compared to that for W, and the fraction of misplaced W's is very small (0.79%), the identification of the associated S position is not as clear as in the MoS_2 case, and so its fractional site occupancy is fixed to be equal to that of the W that is out of place due to the stacking faults.[27,28]

The SXRD patterns from three different planes (0*kl*, *h*0*l*, and *hk*0) in the reciprocal lattice for both compounds are shown in Figure 3. Streaking, which would indicate the presence of a large fraction of stacking faults, is not clearly visible in these reciprocal lattice planes. This is consistent with the small fraction of stacking faults inferred from the structural refinements. Figure 4 contains an illustration of one possible type of stacking fault that would lead to the observed partially occupied sites in MoS_2. The stacking faults as envisioned can be interpreted as an occasional intergrowth of 3R-MoS_2 in an otherwise 2H structure.

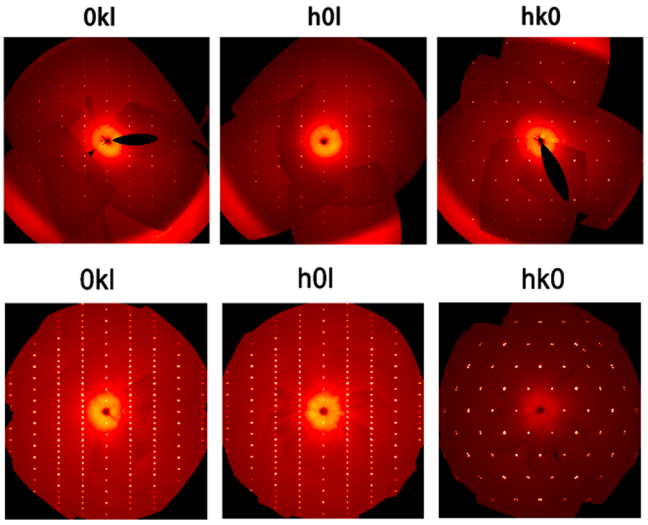

Figure 3. Single-crystal X-ray diffraction characterization of salt-flux-grown MoS_2 and WS2 crystals. Top: Three reciprocal lattice planes (0*kl*, *h*0*l*, and *hk*0) for MoS_2. Bottom: The equivalent patterns for WS_2.

Larger flakes of MoS_2 and WS_2 were inspected using SEM to determine whether they were true single crystals or merely well-defined agglomerations of smaller crystals. Images of two flakes of MoS_2 can be seen in Figure 5, and one flake of WS_2 is in Figure 6. The lack of visible boundaries or seams in the surfaces of the flakes suggests that these samples are single crystals. Small hexagon-like growth features ("islands") can be

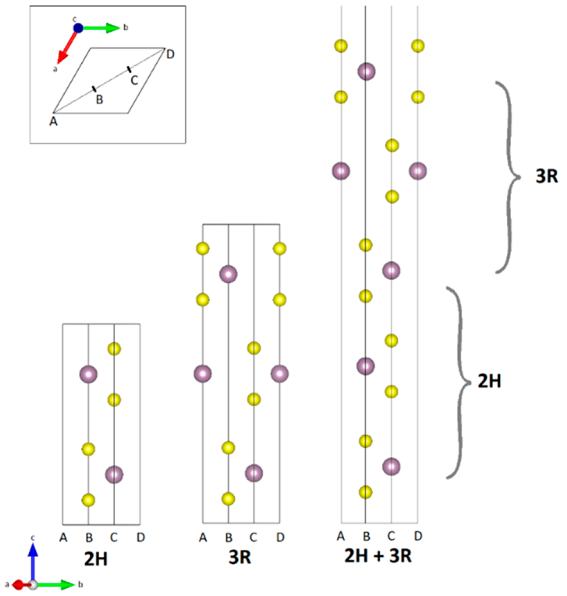

Figure 4. Illustration of one possible origin of the partially occupied Mo and S sites in MoS_2. The structures of pristine 2H-MoS_2[29] and 3R-MoS_2[30] are shown, as well as a demonstration of how the partially occupied sites can arise as a result of stacking faults in the form of a 3R intergrowth in the otherwise 2H structure. Inset: A diagram indicating the projection used.

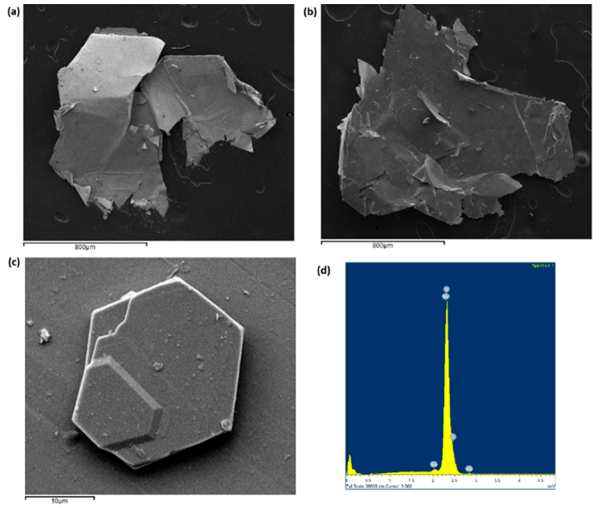

Figure 5. Microscopic characterization of the salt-flux-grown MoS_2 crystals (a) and (b) SEM images of two flakes of MoS_2. (c) SEM image of hexagonal growth feature on surface of flake pictured in (b). (d) EDS spectrum on a small region of feature pictured in (c).

observed on the surfaces of all MoS_2 flakes studied. A close-up image some of these hexagonal features can be seen in Figures 5c and 7b. Figure 5c is of particular interest, as the hexagonal island has itself developed a similar feature on its surface. The flakes of WS_2 do not appear to exhibit the same growth features. EDX measurements on several samples indicate that the flakes are pure MoS_2 and WS_2, respectively, and that no other elements are present in a measurable quantity.

Results from the Sn-based flux growth of MoS_2 from Zhang et al.[18] indicated that their bulkier crystals result from screw-dislocation-driven (SDD) growth. As the mechanism of crystal growth is determined by a number of factors, including subtle differences in chemical potential, it is not necessarily the case

DOI: 10.1021/acs.cgd.9b00785
Cryst. Growth Des. 2019, 19, 5762−5767

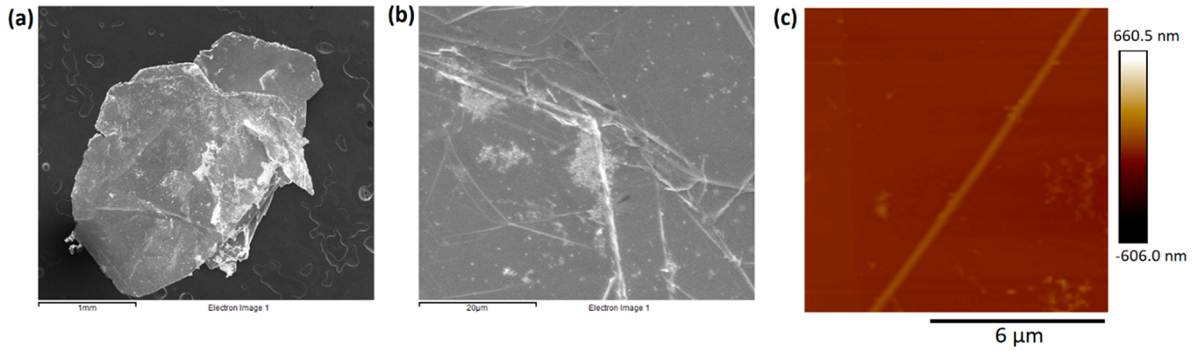

Figure 6. Microscopic characterization of the salt-flux-grown WS_2 crystals (a) SEM image of WS_2 flake. (b) Close-up of surface, showing hexagonal nature of layers but no small island growth features as in MoS_2. (c) AFM image of WS_2 surface, showing a layer edge but no clear indicators of crystal growth mechanism.

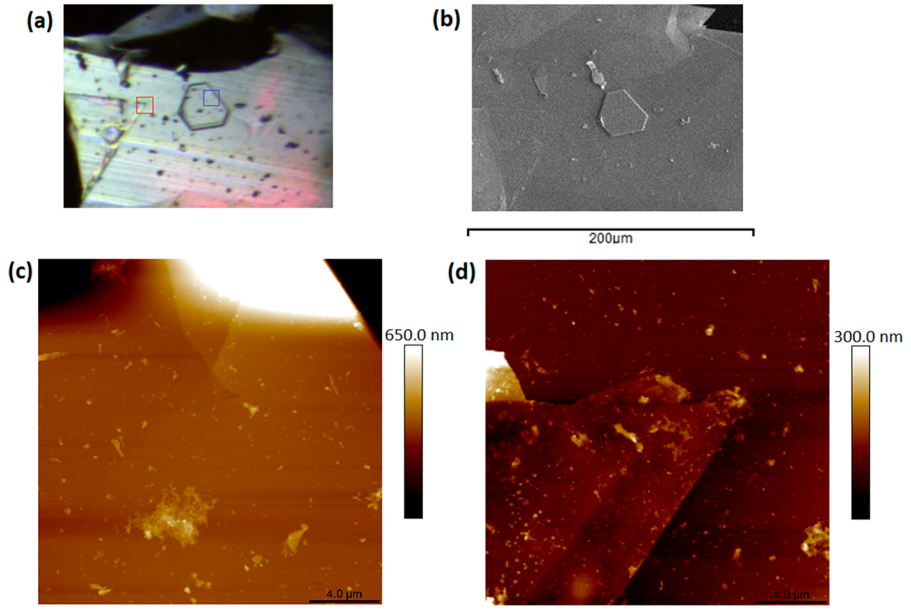

Figure 7. Microscopic characterization of the salt-flux-grown MoS_2 crystals. (a) Optical microscope image of the surface of a MoS_2 flake, showing visible striations across the surface, as well as a hexagonal surface feature. (b) SEM image of the same corresponding region. (c) AFM image of the surface of the hexagonal feature, indicated by the blue box in (a). (d) AFM image of the end of the triangular feature indicated by a red box in (a).

that the same mechanism will apply.[31] In order to compare the growth mechanism of our samples, atomic force microscopy (AFM) measurements were performed on several regions of a single-crystal flake of MoS_2. Figure 7 depicts the results of AFM measurements on two regions of a crystalline flake; Figure 7c shows the surface of one of the hexagonal features, while Figure 7d depicts a striated triangular feature that was observed nearby. Figure 7a,b are optical and SEM images of the broader region, with specific areas of interest identified in Figure 7a by colored boxes. For clarity, Figure 7c was cropped and rotated, but images have otherwise not been manipulated. While striations are visible on the crystal surface, there is no evidence of the spiral-like patterns typically associated with SDD growth. The presence of the hexagonal features on the crystal surface suggests instead that our crystals form via surface nucleation growth, which may explain the thinner nature of our crystals in relation to the bulkier samples of Zhang et al. A flake of WS_2 examined via AFM can be seen in Figure 6c. WS_2 flakes do not display any of the small hexagonal features, nor any of the spiral patterns that are indicative of SDD growth. The precise growth mechanism of these crystals therefore remains ambiguous.

Characterization by Photoluminescence. In order to evaluate the intrinsic optical quality of the solution-transport-grown MoS_2, we prepared monolayers of MoS_2 by exfoliation and encapsulated between thin, insulating hexagonal boron nitride (hBN) on SiO_2 (285 nm)/Si substrate as shown in Figure 8a. Photoluminescence (PL) spectra were taken at T = 4 K on the hBN/MoS_2/hBN heterostructure, as well as on similar heterostructures composed of different MoS_2 crystals available from commercial vendors (HQ graphene and 2D semiconductor). The PL spectra of these heterostructures, shown in Figure 8b, exhibit narrow neutral exciton (X^0) emission at energies between 1.93 and 1.95 eV due to a different dielectric environment, with a line width varying, depending on the sample used and the detection spot position. Notably, the exciton line width of our solution-transport-grown MoS_2 is around 4 meV, comparable to chloride-assisted vapor transport-grown MoS_2[32] and three times sharper than that of either commercial sample (11.5 and 15.5 meV for HQ graphene and 2D semiconductor respectively). This sharper

DOI: 10.1021/acs.cgd.9b00785
Cryst. Growth Des. 2019, 19, 5762−5767

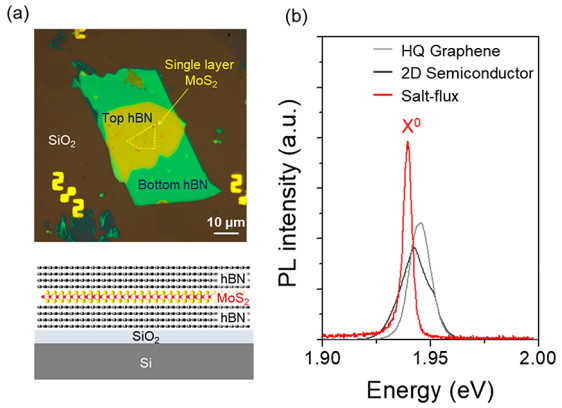

Figure 8. Photoluminescent characterization of the salt-flux-grown MoS_2 crystals. (a) (Top) optical image and (bottom) schematic of MoS_2 monolayer encapsulated between two hBN layers is placed on SiO_2 (285 nm)/Si substrates. The dashed yellow lines show the outline of MoS_2. (b) Photoluminescence spectra at T = 4 K for monolayer MoS_2 encapsulated with hexagonal boron nitride (hBN). The neutral exciton transition exhibits a line width of 4 meV for this solution-transport-grown monolayer MoS_2 (red), which is three times narrower compared to other commercial samples (gray and light gray).

excitonic emission in our monolayer MoS_2 suggests that our growth method can produce high optical quality without a pronounced degree of disorder that can lead to inhomogeneous broadening in the PL spectra.

CONCLUSION

Leaf-like single crystals of MoS_2 and WS_2 have been grown using a liquid-transport flux method, using a CsCl/NaCl eutectic salt in a horizontal configuration. Characterization in a heterostructure device shows that luminescence from the crystals displays a more narrow energy spread than those available commercially. Crystals of WS_2 are also grown by the same method. No clear signs of surface nucleation or screw-dislocation-driven growth are observed. Aside from the sulfide compounds described here, early experiments suggest that this method may also be successfully applied to the growth of single crystals of the related transition metal diselenides WSe_2 and $MoSe_2$.

ASSOCIATED CONTENT

Supporting Information

The Supporting Information is available free of charge on the ACS Publications website at DOI: 10.1021/acs.cgd.9b00785.

Document containing four tables of crystallographic refinements and results for MoS_2 and WS_2, and a powder XRD pattern for MoS_2 (PDF)

Accession Codes

CCDC 1921982 and 1922046 contain the supplementary crystallographic data for this paper. These data can be obtained free of charge via www.ccdc.cam.ac.uk/data_request/cif, or by emailing data_request@ccdc.cam.ac.uk, or by contacting The Cambridge Crystallographic Data Centre, 12 Union Road, Cambridge CB2 1EZ, UK; fax: +44 1223 336033.

AUTHOR INFORMATION

Corresponding Author

*E-mail: fac2@princeton.edu.

ORCID

F. Alex Cevallos: 0000-0002-3459-0091
Shu Guo: 0000-0002-2098-8904
Giovanni Scuri: 0000-0003-1050-3114
Philip Kim: 0000-0002-8255-0086
Hongkun Park: 0000-0001-9576-8829

Notes

The authors declare no competing financial interest.

ACKNOWLEDGMENTS

This research was supported by the Gordon and Betty Moore Foundation EPiQS initiative, Grants GBMF-4412 and GBMF-4543. H.P. acknowledges support from the DoD Vannevar Bush Faculty Fellowship (N00014-16-1-2825).

REFERENCES

(1) Manzeli, S.; Ovchinnikov, D.; Pasquier, D.; Yazyev, O. V.; Kis, A. 2D transition metal dichalcogenides. *Nat. Rev. Mater.* **2017**, *2*, 17033.
(2) Nagata, S.; Aochi, T.; Abe, T.; Ebisu, S.; Hagino, T.; Seki, Y.; Tsutsumi, K. Superconductivity in the layered compound 2H-TaS_2. *J. Phys. Chem. Solids* **1992**, *53*, 1259−1263.
(3) Kusmartseva, A. F.; Sipos, B.; Berger, H.; Forro, L.; Tutis, E. Pressure Induced Superconductivity in Pristine 1T-$TiSe_2$. *Phys. Rev. Lett.* **2009**, *103*, 236401.
(4) Qi, Y.; Naumov, P. G.; Ali, M. N.; Rajamathi, C. R.; Schnelle, W.; Barkalov, O.; Hanfland, M.; Wu, S.-C.; Shekhar, C.; Sun, Y.; Suß, V.; Schmidt, M.; Schwarz, U.; Pippel, E.; Werner, P.; Hillebrand, R.; Forster, T.; Kampert, E.; Parkin, S.; Cava, R. J.; Felser, C.; Yan, B.; Medvedev, S. A. Superconductivity in Weyl semimetal candidate $MoTe_2$. *Nat. Commun.* **2016**, *7*, 11038.
(5) Albertini, O. R.; Zhao, R.; McCann, R. L.; Feng, S.; Terrones, M.; Freericks, J. K.; Robinson, J. A.; Liu, A. Y. Zone-center phonons of bulk, few-layer, and monolayer 1T-TaS_2: Detection of commensurate charge density wave phase through Raman scattering. *Phys. Rev. B: Condens. Matter Mater. Phys.* **2016**, *93*, 214109.
(6) Barja, S.; Wickenburg, S.; Liu, Z.-F.; Zhang, Y.; Ryu, H.; Ugeda, M. M.; Hussain, Z.; Shen, Z.-X.; Mo, S.-K.; Wong, E.; Salmeron, M. B.; Wang, F.; Crommie, M. F.; Ogletree, D. F.; Neaton, J. B.; Weber-Bargioni, A. Charge density wave order in 1D mirror twin boundaries of single-layer $MoSe_2$. *Nat. Phys.* **2016**, *12*, 751−756.
(7) Amani, M.; Burke, R. A.; Ji, X.; Zhao, P.; Lien, D.-H.; Taheri, P.; Ahn, G. H.; Kirya, D.; Ager, J. W.; Yablonovitch, E.; Kong, J.; Dubey, M.; Javey, A. High Luminescence Efficiency in MoS_2 Grown by Chemical Vapor Deposition. *ACS Nano* **2016**, *10*, 6535−6541.
(8) Splendiani, A.; Sun, L.; Zhang, Y.; Li, T.; Kim, J.; Chim, C.-Y.; Galli, G.; Wang, F. Emerging Photoluminescence in Monolayer MoS_2. *Nano Lett.* **2010**, *10*, 1271−1275.
(9) Zong, X.; Wu, G.; Yan, H.; Ma, G.; Shi, J.; Wen, F.; Wang, L.; Li, C. Photocatalytic H_2 Evolution on MoS_2/CdS Catalysts under Visible Light Irradiation. *J. Phys. Chem. C* **2010**, *114*, 1963−1968.
(10) Qiao, X.-Q.; Zhang, Z.-W.; Tian, F.-Y.; Hou, D.-F.; Tian, Z.-F.; Li, D.-S.; Zhang, Q. Enhanced Catalytic Reduction of *p*-Nitrophenol on Ultrathin MoS_2 Nanosheets Decorated with Noble Metal Nanoparticles. *Cryst. Growth Des.* **2017**, *17*, 3538−3547.
(11) Jin, C.; Regan, E. C.; Yan, A.; Utama, M. I. B.; Wang, D.; Zhao, S.; Qin, Y.; Yang, S.; Zheng, Z.; Shi, S.; Watanabe, K.; Taniguchi, T.; Tongay, S.; Zettl, A.; Wang, F. Observation of moiré excitons in WSe_2/WS_2 heterostructure superlattices. *Nature* **2019**, *567*, 76−80.
(12) Liu, K.-K.; Zhang, W.; Lee, Y.-H.; Lin, Y.-C.; Chang, M.-T.; Su, C.-Y.; Chang, C.-S.; Li, H.; Shi, Y.; Zhang, H.; Lai, C.-S.; Li, L.-J. Growth of Large-Area and Highly Crystalline MoS_2 Thin Layers on Insulating Substrates. *Nano Lett.* **2012**, *12*, 1538−1544.
(13) Chen, W.; Zhao, J.; Zhang, J.; Gu, L.; Yang, Z.; Li, X.; Yu, H.; Zhu, X.; Yang, R.; Shi, D.; Lin, X.; Guo, J.; Bai, X.; Zhang, G. Oxygen-Assisted Chemical Vapor Deposition Growth of Large Single-Crystal and High-Quality Monolayer MoS_2. *J. Am. Chem. Soc.* **2015**, *137*, 15632−15635.

DOI: 10.1021/acs.cgd.9b00785
Cryst. Growth Des. 2019, 19, 5762−5767

(14) Al-Hilli, A. A.; Evans, B. L. The preparation and properties of transition metal dichalcogenide single crystals. *J. Cryst. Growth* **1972**, *15*, 93−101.
(15) Hong, J.; Hu, Z.; Probert, M.; Li, K.; Lv, D.; Yang, X.; Gu, L.; Mao, N.; Feng, Q.; Xie, L.; Zhang, J.; Wu, D.; Zhang, Z.; Jin, C.; Ji, W.; Zhang, X.; Yuan, J.; Zhang, Z. Exploring atomic defects in molybdenum disulphide monolayers. *Nat. Commun.* **2015**, *6*, 6293.
(16) Pisoni, A.; Jacimovic, J.; Barisic, O. S.; Walter, A.; Nafradi, B.; Bugnon, P.; Magrez, A.; Berger, H.; Revay, Z.; Forro, L. The Role of Transport Agents in MoS_2 Single Crystals. *J. Phys. Chem. C* **2015**, *119*, 3918−3922.
(17) Addou, R.; McDonnell, S.; Barrera, D.; Guo, Z.; Azcatl, A.; Wang, J.; Zhu, H.; Hinkle, C. L.; Quevedo-Lopez, M.; Alshareef, H. N.; Colombo, L.; Hsu, J. W. P.; Wallace, R. M. Impurities and Electronic Property Variations of Natural MoS_2 Crystal Surfaces. *ACS Nano* **2015**, *9*, 9124−9133.
(18) Zhang, X.; Lou, F.; Li, C.; Zhang, X.; Jia, N.; Yu, T.; He, J.; Zhang, B.; Xia, H.; Wang, S.; Tao, X. Flux Method Growth of Bulk MoS_2 Single Crystals and Their Application as a Saturable Absorber. *CrystEngComm* **2015**, *17*, 4026−4032.
(19) McCarroll, W. H.; Greenblatt, M. Preparation of Lithium Molybdenum Oxide Bronzes by a Temperature Gradient Flux Growth Technique. *J. Solid State Chem.* **1984**, *54*, 282−290.
(20) Böhmer, A. E.; Hardy, F.; Eilers, F.; Ernst, D.; Adelmann, P.; Schweiss, P.; Wolf, T.; Meingast, C. Lack of coupling between superconductivity and orthorhombic distortion in stoichiometric single-crystalline FeSe. *Phys. Rev. B: Condens. Matter Mater. Phys.* **2013**, *87*, No. 280505(R).
(21) Chareev, D. A. General principles of the synthesis of chalcogenides and pnictides in salt melts using a steady-state temperature gradient. *Crystallogr. Rep.* **2016**, *61*, 506−511.
(22) Yan, J.-Q.; Sales, B. C.; Susner, M. A.; McGuire, M. A. Flux growth in a horizontal configuration: An analog to vapor transport growth. *Phys. Rev. Mater.* **2017**, *1*, 023402.
(23) Sheldrick, G. M. Crystal structure refinement with SHELXL. *Acta Crystallogr., Sect. C: Struct. Chem.* **2015**, *71*, 3−8.
(24) Dolomanov, O. V.; Bourhis, L. J.; Gildea, R. J.; Howard, J. A. K.; Puschmann, H. OLEX2: a complete structure solution, refinement and analysis program. *J. Appl. Crystallogr.* **2009**, *42*, 339−341.
(25) Spek, A. L. J.; Spek, A. L. Single-crystal structure validation with the program PLATON. *J. Appl. Crystallogr.* **2003**, *36*, 7−13.
(26) Zomer, P. J.; Guimarães, M. H. D.; Brant, J. C.; Tombros, N.; van Wees, B. J. Fast pick up technique for high quality heterostructures of bilayer graphene and hexagonal boron nitride. *Appl. Phys. Lett.* **2014**, *105*, 013101.
(27) MoS_2 crystal structure information. Occupancy of each site: Mo1 (2*c*): 0.9686(14). Mo2 (2*b*): 0.0314(14). S1 (4*f*): 0.9686(14). S2 (4e): 0.0314(14). Formula mass: 160.06 amu. Crystal system: hexagonal. Space group: $P6_3/mmc$. Unit cell dimensions: a = 3.1601(10) Å, c = 12.288(4) Å, V = 106.27(6) Å^3. T = 300(1) K. Z = 2. μ = 7.648 mm^{-1}. Final R Indices ($R_1/\omega R_1$) = 0.0144/0.0367.
(28) WS_2 crystal structure information. Occupancy of each site: W1 (2*c*): 0.9921(12). W2 (2*b*): 0.0079(12). S1 (4*f*): 0.99. S2 (4e): 0.01. Formula mass: 247.98 amu. Crystal system: hexagonal. Space group: $P6_3/mmc$. Unit cell dimensions: a = 3.1599(4) Å, c = 12.3554(17) Å, V = 106.84(2) Å^3. T = 300(1) K. Z = 2. μ = 55.530 mm^{-1}. Final R indices ($R_1/\omega R_1$) = 0.0119/0.0247.
(29) Petkov, V.; Billinge, S. J. L.; Larson, P.; Mahanti, S. D.; Vogt, T.; Rangan, K. K.; Kanatzidis, M. G. Structure of nanocrystalline materials using atomic pair distribution function analysis: study of $LiMoS_2$. *Phys. Rev. B: Condens. Matter Mater. Phys.* **2002**, *65*, 0921051−0921054.
(30) Takeuchi, Y.; Nowacki, W. Detailed crystal structure of rhombohedral MoS_2 and systematic deduction of possible polytypes of molybdenite. *Schweiz. Mineral. Petrogr. Mitt.* **1964**, *44*, 105−120.
(31) Uwaha, M. Growth Kinetics: Basics of Crystal Growth Mechanisms. In *Handbook of Crystal Growth*, 2nd ed.; Nishinaga, T., Ed.; Elsevier, 2015; pp 359−399.
(32) Cadiz, F.; Courtade, E.; Robert, C.; Wang, G.; Shen, Y.; Cai, H.; Taniguchi, T.; Watanabe, K.; Carrere, H.; Lagarde, D.; Manca, M.; Amand, T.; Renucci, P.; Tongay, S.; Marie, X.; Urbaszek, B. Excitonic Linewidth Approaching the Homogenous Limit in MoS_2-Based van der Waal Heterostructure. *Phys. Rev. X* **2017**, *7*, 021026.

DOI: 10.1021/acs.cgd.9b00785
Cryst. Growth Des. 2019, 19, 5762−5767